



# Documentation for the 2002 Update of the National Seismic Hazard Maps

by Arthur D. Frankel<sup>1</sup>, Mark D. Petersen<sup>1</sup>, Charles S. Mueller<sup>1</sup>,  
Kathleen M. Haller<sup>1</sup>, Russell L. Wheeler<sup>1</sup>, E.V. Leyendecker<sup>1</sup>,  
Robert L. Wesson<sup>1</sup>, Stephen C. Harmsen<sup>1</sup>, Chris H. Cramer<sup>2</sup>,  
David M. Perkins<sup>1</sup>, and Kenneth S. Rukstales<sup>1</sup>

Open-File Report 02-420

2002

This report is preliminary and has not been reviewed for conformity with the U.S. Geological Survey editorial standards or with the North American Stratigraphic Code. Any use of trade, firm or product names is for descriptive purposes only and does not imply endorsement by the U.S. Government.

U.S. DEPARTMENT OF THE INTERIOR  
U.S. GEOLOGICAL SURVEY

<sup>1</sup> Denver, Colorado

<sup>2</sup> Memphis, Tennessee

## Introduction

We have produced updated seismic hazard maps for the conterminous United States, based on new seismological, geophysical, and geological information. The 2002 maps contain important changes from the previous version of the national seismic hazard maps made in 1996. However, most of these changes are incremental. For the 1996 maps, we developed a new methodology quite different from that used in prior USGS national seismic hazard maps (see Frankel et al., 1996; Frankel et al., 2000). In addition, we instituted an open, consensus-building process where there was feedback from geoscientists and engineers on the methodology and inputs for the maps during several regional workshops. The development of the 2002 maps followed the same open process.

Many of the changes in the 2002 maps were suggested by participants in four regional workshops that we held: Pacific Northwest (Seattle, March, 2000), Central and Eastern U.S. (St. Louis, June 2000), California (Pasadena, Sept. 2000), and Intermountain West (Salt Lake City, March, 2001). Modifications to the maps were also discussed in a user workshop convened by the Applied Technology Council (ATC) and the USGS in May 2001.

Draft maps were placed on our website ([geohazards.cr.usgs.gov/eq/](http://geohazards.cr.usgs.gov/eq/)) in January and August 2002 for comment. We requested review of the fault parameters from the western state geological surveys. Most of them provided comments. An external panel of non-USGS experts has also reviewed the maps and provided feedback during two meetings with project staff. The finalized maps presented here reflect many changes based on the comments we received on the draft maps.

The 2002 maps constructed to date are for peak ground acceleration (PGA), and 0.2 sec and 1.0 sec spectral acceleration (for 5% damping) at 10% and 2% probabilities of exceedance (PE) in 50 years (see Appendix B). We will also calculate spectral accelerations at periods of 0.1, 0.3, 0.5, 1.0 and 2.0 sec and will release uniform hazard spectra and hazard curves, as we did for the 1996 maps. The hazard maps are for a firm-rock site condition, where the shear-wave velocity averaged over the top 30m ( $V_{s30}$ ) is 760 m/s (boundary of NEHRP site classes B and C).

The description below focuses on changes from the 1996 maps. The general methodology and organizing principles for the 2002 update are the same as the 1996 maps (see Frankel et al., 1996; available on our website). We typically use a combination of hazard curves calculated from gridded spatially-smoothed seismicity (see Frankel, 1995), large background zones, and specific fault sources. In some cases, areal zones with seismicity rates constrained by GPS deformation data are applied.

The California portion of the maps was produced jointly by the USGS and the California Geological Survey. The methodology for the 1996 maps for California is described in more detail in Petersen et al. (1996).

Throughout the revision, we have included more explicit treatment of uncertainties. In most cases we use the mean recurrence times, since we are first concerned with producing mean hazard maps. Therefore, it is not necessary to do a logic tree of recurrence rate when constructing a mean hazard map. We intend to produce maps of uncertainties after the maps derived from the mean hazard curves.

Our earthquake catalog was updated to include earthquakes through December 2001 and new seismicity grids constructed after dependent events were removed. In all regions, we made a more extensive effort for the 2002 maps to remove quarry blasts and other explosions from the earthquake catalog before calculating the seismicity parameters. For example, we removed blasts for the Kentucky catalog using the report of Street et al. (2002). In other cases we used additional information from the National Earthquake Information Center to identify suspected blasts in the catalog.

### Central and Eastern U.S. (CEUS)

The changes that most affect the CEUS portion of the maps are: 1) changes in mean recurrence time, characteristic magnitude, and spatial concentration of New Madrid sources of large earthquakes, 2) changes in mean recurrence time and spatial concentration of Charleston, SC source of large earthquakes, and 3) incorporation of additional attenuation relations.

#### New Madrid Region

The 2002 update incorporates a shorter mean recurrence time for characteristic earthquakes in New Madrid than was used in the 1996 maps, as well as a smaller median magnitude than that applied in 1996. A logic tree was developed for the characteristic magnitude ( $M_{char}$ ) and the configuration of the sources of the characteristic earthquakes, where the uncertainty in location is described by using three fictitious fault sources as in the 1996 maps. A mean recurrence time of 500 years for characteristic earthquakes is used in the calculations (see Cramer, 2001). This was based on the paleoliquefaction evidence of two to three previous sequences prior to the 1811-12 events (Tuttle and Schweig, 2000). In the 1996 maps, we used a 1000 year mean recurrence time for moment magnitude 8.0 earthquakes.

A logic tree for  $M_{char}$  for the New Madrid area was developed using input from the CEUS workshop (Wheeler and Perkins, 2000) and recent work by Bakun and Hopper (2002) on the magnitudes of the 1811-12 New Madrid sequence. Using a new method for evaluating magnitude by directly inverting observations of intensities, Bakun and Hopper (2002) determined a moment magnitude  $M$  of 7.4 (7.0-7.7 at 95% confidence level) for the largest New Madrid earthquake in the 1811-12 sequence. This value is significantly lower than the  $M$ 8.0 magnitude determined by Johnston (1996a) from isoseismal areas. Hough et al. (2000) also estimated lower magnitudes for the 1811-12 sequence than Johnston (1996a), after adjusting intensities for site amplification.

The  $M_{char}$  logic tree used in the 2002 maps for New Madrid is:  $M$ 7.3 (0.15 wt),  $M$ 7.5 (0.2 wt),  $M$ 7.7 (0.5 wt),  $M$ 8.0 (0.15 wt). This logic tree is meant to characterize the current range of expert opinion on the magnitude of the largest events of the 1811-12 sequence (see Wheeler and Perkins, 2000), with the lowest magnitude branch encompassing the Bakun and Hopper (2002) magnitude estimate and the highest magnitude derived from the estimate of Johnston (1996a). We found that incorporating this logic tree produced essentially the same mean hazard as giving full weight to the  $M$  7.7 scenario. The  $M$ 7.7 choice may be bolstered by the similarity in the isoseismals

with distance between the 2001 Bhuj India earthquake (measured **M** 7.6-7.7) and those of the 16 Dec 1811 New Madrid event (Bendick et al., 2001), although Bakun and McGarr (2002) find differing rates of attenuation of intensities for the eastern U.S. and India. As the new Bakun and Hopper (2002) work on magnitudes from intensities is assessed by the seismological community, the weights assigned to the logic-tree branches may need revision in future national maps.

At the CEUS workshop, there was general sentiment for a more concentrated source for the characteristic events than the three equally weighted “fictitious sources” used in the 1996 maps (Wheeler and Perkins, 2000). These three sources consisted of a fault trace matching the recent microearthquake activity and two adjacent sources that are situated near the borders of the Reelfoot Rift (see Figure 1). For the 2002 maps, we therefore gave higher weight to the center fault used in 1996. This center fault was given twice the weight of each of the faults to the side. Thus, the effective rates (after weighting) used were  $1.0\text{e-}3$  per year for the center fault and  $5.0\text{e-}4$  per year for each side fault. The total rate equals  $1/500$  yr. It is important to note that the probabilistic ground motions for the 10% probability of exceedance level have increased markedly around the New Madrid area, compared to the 1996 maps. This is caused by the shorter mean return time of 500 years for characteristic earthquakes used in the 2002 maps.

#### Charleston, South Carolina

We used a mean recurrence time of 550 years for characteristic earthquakes in the Charleston, South Carolina region, as presented in the description of paleoseismic evidence by Talwani and Schaeffer (2001). This average recurrence time is derived from the recurrence intervals determined from the 1886 event and 3 earlier earthquakes of similar size as evidenced by the areal extent of their paleoliquefaction effects. For the 1996 maps, we used a recurrence time of 650 years for a **M**7.3 earthquake. In the 1996 maps, a relatively large source zone was used for the characteristic earthquake. The CEUS workshop participants preferred a more concentrated zone following the Woodstock lineament and a portion of the zone of river anomalies (Wheeler and Perkins, 2000). We assigned a half weight to the broad zone used in 1996 and half weight to the narrower zone. Figures 2 and 3 depict the two source zones. The use of the narrower source zone causes an increase in probabilistic ground motions within this narrow zone and a decrease in ground motions in a halo around this narrow zone, compared to the 1996 maps.

When implementing the areal zones, our program divides the zone into grid cells 0.1 degree on a side. The rate of earthquakes in the zone is divided up into a rate for each cell. In the distance calculation to the site, each cell is used as the center of a fault. For both areal zones, the faults are oriented with strikes parallel to the bng axis of the narrow areal zone. Fault lengths are determined from Wells and Coppersmith (1994). Note that some of the faults extend outside of the source zone boundary.

The logic tree we used for characteristic magnitude of Charleston-type earthquakes was **M** 6.8 (0.2 wt), **M** 7.1 (0.2 wt), **M**7.3 (0.45 wt), and **M** 7.5 (0.15 wt). This was based on the range in expert opinion gathered at our CEUS workshop, with the lowest branch added to accommodate the more recent work of Bakun and Hopper (2002). They find a preferred moment magnitude of 6.8 for the 1886 event, with a 95%

confidence interval of **M** 6.4-7.1. The CEUS workshop preferred a median magnitude of 7.3, based on the work of Johnston (1996a).

#### Other Source Changes for CEUS

Figure 4 shows the revised **M**<sub>max</sub> zones used for the calculation of the hazard from the gridded seismicity for the 2002 maps. The **M**<sub>max</sub> 7.5 zone assigned to the Wabash Valley area was enlarged to include the most likely rupture zones from paleoearthquakes with magnitudes above about 7.0 (Wheeler and Cramer, 2002). The extended-margin **M**<sub>max</sub> and background seismicity zone was slightly enlarged to include the Rough Creek Graben and Rome Trough. The **M**<sub>max</sub> of the inboard “craton” zone was increased to **M** 7.0 from the 6.5 value used in 1996. The value of 7.0 was overwhelmingly suggested by the CEUS workshop participants, based on the global survey of stable continental regions by Johnston et al. (1994).

We used Johnston (1996b) and Boore and Atkinson (1987) mblg to **M** conversions as separate branches of a logic tree (with equal weight) for the calculation of hazard from the gridded seismicity. Such a conversion is applied (a) in implementing the attenuation relations when they are given in **M**, (b) in finding the mblg max from **M**<sub>max</sub>, and (c) in determining fault lengths in the finite fault calculation for the gridded seismicity.

In the gridded seismicity hazard calculation for magnitudes above 6.0 we used finite faults centered on each grid cell. The length of each fault is determined from Wells and Coppersmith (1994). The faults have random strikes. A similar procedure was used for the WUS in the 1996 and 2002 maps. We have applied this to the CEUS for the 2002 maps, although it makes almost no difference to the ground-motion maps for 2% PE in 50 years and higher probabilities. This procedure has more effect on the lower probability levels.

Another change in the updated maps is the weighting assigned for the background zone in the Rocky Mountain region, which is in the CEUS attenuation region for the maps. In the 1996 maps, an adaptive weighting scheme was applied such that the background zones for the CEUS were given a weight of 0.2 for those grid cells in which the spatially-smoothed historic seismicity rate was lower than the seismicity rate for that cell derived from the historic seismicity rate of the background zone. The models from the spatially-smoothed seismicity were given a total of 0.8 weight for these cases and full weight otherwise. This procedure provides a hazard floor where historical seismicity was low. This adaptive weighting scheme caused an apparent embayment of lower hazard in northern Colorado (compared to western Colorado), even though this is the area where the **M** approximately 6.5 earthquake occurred in 1882 (Spence et al., 1996). This apparent embayment of hazard is caused by the higher hazard estimates to the southwest and north caused by the more numerous magnitude 3 and 4 earthquakes in those areas. For the 2002 maps, we assigned a weight of 1.0 for the Rocky Mountain background zone in areas where the gridded seismicity rate was lower than the background rate, in effect replacing the smoothed seismicity rate with the background rate. This causes a modest increase (about 10%) in the probabilistic ground motions along the Front Range of Colorado and generally aligns the ground motion contours parallel to the Front Range (approximately north-south). We justify the

special treatment for the Rocky Mountain zone by noting the short record of historic seismicity in this region and the attendant high uncertainty in hazard estimates.

We included the 1981 M4 earthquake near Rocky Mountain Arsenal in the catalog for the 2002 maps. We had excluded this event in previous versions of the maps, because the deep fluid injection that caused the swarm of earthquakes at the Arsenal in the 1960's has been terminated. The swarm events near the Arsenal were removed from the catalog for the hazard maps, since the rate of these events is probably not representative of the long-term rate of earthquakes in this area that exists in the absence of fluid injection. However, the occurrence of the 1981 event so long after the termination of injection may imply that the occurrence of this earthquake reflects the long-term seismicity rate for this area (V. Matthews, pers. comm., 2001). The addition of this single earthquake to the catalog made only a very minor change in the hazard maps. We also removed induced earthquakes in the Paradox Valley of western Colorado.

### CEUS Attenuation Relations

Significant differences between the 1996 and 2002 maps are caused by the inclusion of additional attenuation relations in the 2002 maps. In 1996, we used the attenuation relations of Toro et al. (1997) and Frankel et al. (1996), which were assigned equal weight. For the 2002 maps we have added the attenuation relations of Atkinson and Boore (1995), Somerville et al. (2001) and Campbell (2002). All three of these relations have been adjusted to BC site condition using the factors given in Frankel et al. (1996). The Somerville et al (2001) relations were used for the characteristic earthquakes at New Madrid and Charleston, but not for the smoothed seismicity calculations. This relation gives much lower ground motions than the other relations for earthquakes between about magnitude 5 and 6. Since this relation is based on a finite-fault model, it may not be appropriate for these smaller events. We give lower weight to Somerville et al. (2001) and Campbell (2002), because these relations are new and haven't been widely assessed by the seismological community. We think it is important to include these relations in the new maps, because each brings novel and important aspects to the problem. Somerville et al. (2001) uses an extended source model. Campbell (2002) applies a hybrid method of converting empirical WUS attenuation relations using CEUS path and source parameters.

For the 2002 maps, the attenuation relations and weights for the gridded seismicity hazard calculations are: Toro et al. (1997; 0.286 wt), Frankel et al. (1996; 0.286 wt), Atkinson and Boore (1995; 0.286 wt), and Campbell (2002; 0.143 wt). For the characteristic earthquakes (New Madrid and Charleston), the attenuation relations and weights are: Toro et al. (0.25 wt), Frankel et al. (0.25 wt), Atkinson and Boore (0.25 wt), Campbell (0.125 wt), and Somerville et al. (0.125 wt). All relations are adjusted, as in earlier maps, to correspond to the B-C boundary site condition (firm rock,  $V_{s30} = 760$  m/s). We used a table version of the Atkinson and Boore (1995) model calculated by D.M. Boore (written comm., 2002), that directly incorporates site amplifications calculated for the velocity profile used for the BC boundary site condition (see Frankel et al., 1996).

The most significant change in the maps due to the new CEUS attenuation relations is for the 1 Hz spectral acceleration (S.A.). In the extended margin Mmax zone along the Atlantic seaboard, the 1 Hz S.A. values for 2% probability of exceedance in 50 years have decreased by about 20% compared to the 1996 maps. This is caused by the relatively low 1 Hz S.A. values in Atkinson and Boore (1995), which developed a source model with two corner frequencies rather than the single corner frequency models in the Frankel et al. (1996) and Toro et al. (1997) relations applied in the 1996 maps. Decreases for PGA and 0.2 sec S.A. in the 2002 maps for the Atlantic seaboard are much less pronounced (about 10%). There is little change for the probabilistic ground motions at 2% probability of exceedance in 50 years for most of the central U.S.

As in the 1996 CEUS maps, the median ground motions at higher frequencies were truncated to avoid the very large ground motions predicted for the BC site condition. This only affects the hazard maps close to the New Madrid and the Charleston source areas. We capped the median PGA at 1.5g and the 0.2 sec SA at 3.0g. We also truncated the distribution of ground motions at 3 standard deviations ( $\sigma$ ) for all the periods. Furthermore, the ground motion distribution for PGA was truncated at 3.0g and for 0.2 sec SA at 6.0g, when these values were less than the  $3\sigma$  cutoff. These values were chosen to avoid unphysically large ground motions.

### **Western U.S. (WUS)**

The changes that most affect the WUS maps are: 1) changes in fault recurrence parameters for specific faults, 2) changes in the rupture zone geometry and weighting for the Cascadia subduction zone, and 3) addition of new attenuation relations. The latter two changes have caused decreases of the probabilistic ground motions compared to the 1996 maps. Figure 5 shows the faults used in the 2002 maps. Approximately twenty faults have been added since the 1996 maps. The slip rates of all of the faults have been re-examined. The slip rates of some faults have been revised based on new information (see below). These changes will be described in detail in separate documentation.

Characteristic magnitudes were determined from the fault area for California faults and from fault length for other faults. Fault area was not used to determine magnitude for faults outside of California, since there is usually insufficient seismicity in these areas to adequately define the width of these faults. When calculating magnitude from fault length, we used the Wells and Coppersmith (1994) relation for all fault types, rather than the relation for individual fault types (e.g., normal or thrust). The relations for individual fault types were derived from a small number of faults and may overestimate the magnitude of normal fault earthquakes at the larger fault lengths. In a few cases this change caused a decrease of 0.1 magnitude unit (m.u.) in the Mchar estimate for normal faults, compared to the values derived from their “normal faulting” relation.

Characteristic magnitudes were determined from the fault area for California faults, using the relations of Wells and Coppersmith (1994) when the fault area was less than about 500 km<sup>2</sup> and the relations of Ellsworth (in Working Group on California

Earthquake Probabilities [WGCEP], 2002) and Hanks and Bakun (2002) for faults with larger areas. This follows the procedure of the Working Group on California Earthquake Probabilities. The hazard curves from the Ellsworth and Hanks and Bakun (2002) magnitude-area relations were weighted equally.

The weighting of characteristic and truncated Gutenberg-Richter recurrence models for faults in California was revised for 2002. For B-type faults (see Petersen et al. 2000) in California, we used a weighting of 0.67 for the characteristic model and 0.33 for a truncated Gutenberg-Richter model. For other western U.S. B-type faults, we used equal weighting for the characteristic and Gutenberg-Richter models, as in 1996. The use of the truncated GR model is meant to address the possibility that poorly studied faults may be segmented and may not rupture their entire length as implied in the characteristic model. The frequency-magnitude relation of a fault with multiple segments, where there is some probability of rupture crossing each segment, is similar to the GR relation over a limited magnitude range. We assigned lower weight to the GR model for California faults, since these faults have, in general, been studied more than faults in other parts of the WUS. A-type faults were treated as purely characteristic, although we often allow for single and multiple-segment rupture (see below). The Wasatch Fault was assigned a 90% weight for characteristic and 10% weight for truncated Gutenberg-Richter (see below).

In the 2002 maps, we used a b-value of 0.8 for the California calculations, rather than 0.9 as in 1996. We found that the b-value of 0.8 fit the historical seismicity catalog, when aftershocks were removed. As in the 1996 maps, a b-value of 0.8 was used for the rest of the area in the western U.S. attenuation region.

### Uncertainty in Mchar

For most faults we included uncertainties in characteristic magnitude Mchar (which is also Mmax for the Gutenberg-Richter model for faults) when determining recurrence rates for the hazard calculation. Two forms of uncertainty were considered: epistemic (model uncertainty) and aleatory (randomness). We assumed a standard deviation of Mchar of 0.24 magnitude units and split this equally into epistemic and aleatory uncertainties.

A logic tree was used to characterize the epistemic uncertainty about Mchar, the magnitude determined from the Wells and Coppersmith (1994) relation of magnitude versus surface rupture length or from the Ellsworth (in WGCEP 2002) and Hanks and Bakun (2002) relations of magnitude versus fault area. In the logic tree, we assigned a weight of 0.6 to Mchar, a weight of 0.2 to Mchar +0.2 and a weight of 0.2 to Mchar - 0.2. For each branch the recurrence rate was calculated so that the moment rate equaled the rate from the mean slip rate and the original Mchar. For the southern San Andreas fault, the logic tree consisted of Mchar-0.1, Mchar, and Mchar+0.1, since we did not want the magnitude of the M8.1 scenario that ruptures the entire southern San Andreas to get too large (see Appendix A).

We used the same logic tree to characterize the epistemic uncertainty of Mmax for the truncated Gutenberg-Richter (GR) model for fault recurrence, which is the same as Mchar. Again, the moment rate was balanced for each branch of the logic tree.

For the characteristic recurrence model, each branch of the logic tree was assigned a distribution of magnitudes for the aleatory uncertainty. This was a normal distribution with a standard deviation of 0.12 magnitude units. The distribution was truncated at  $\pm 0.15$  magnitude units, so that characteristic magnitudes would not get too far from the original magnitude estimate. The recurrence rates for each magnitude in the distribution were determined so that the moment rate sum for the distribution of that branch equaled the moment rate based on  $M_{char}$  and the mean slip rate.

We found that including epistemic uncertainty slightly increases the probabilistic ground motions derived from the mean hazard curves and including aleatory uncertainty slightly decreases these motions. Including both results in little change in the ground motions derived from the mean hazard curves, compared to the case of just using the mean slip rate and  $M_{char}$ .

When the lowest magnitude point of the distribution on the lowest magnitude branch of the logic tree was less than  $M_{5.8}$ , we did not include the aleatory and epistemic uncertainty for the characteristic model. When the lowest magnitude branch of the logic tree was less than or equal to  $M_{6.5}$ , we did not include the uncertainty in the GR model. This  $M_{6.5}$  limit for the GR model was the minimum magnitude used in the GR calculation.

## California Issues

Many changes have been made in the fault parameters used in California. These will be described in a document being prepared by the California Geological Survey.

The 2002 maps use a set of runs for major faults in the San Francisco Bay region specified by the Working Group on California Earthquake Probabilities (WGCEP, 2002). The Working Group conducted an extensive expert-opinion study to develop distributions of recurrence times and magnitudes of large earthquakes on the major faults in the region. Realizations of magnitude and recurrence time for each fault were supplied by the Working Group, based on Monte Carlo sampling of the distributions used in their study. We used these realizations to determine mean rates of occurrence on each fault for each magnitude bin. As with the other aspects of the national maps, we used the mean hazard curves to derive the probabilistic ground motions for the maps.

For the southern San Andreas fault, we completely changed the multiple-segment scenarios used in the 1996 maps. We now apply two new models, each with 0.5 weight. These models produced very similar hazard maps for PGA with 2%PE in 50 years. The models are described in Appendix A.

For 2002, we explicitly included the creeping section of the San Andreas fault. Based on historic seismicity, we used a magnitude 6.2 earthquake on the creeping section with a recurrence rate of 0.0165 per year. In addition, we calculated the hazard from  $M_{5.0-6.0}$  from spatially smoothing the historical seismicity. First we extracted events within 20 km of the creeping section of the fault. We then used an anisotropic smoothing function to smooth the seismicity rate grid calculated from these epicenters. The correlation distance was 75 km along the fault strike and 10 km perpendicular to the strike. When calculating the hazard from the gridded seismicity we fixed the fault strike to the observed strike of the San Andreas fault. When calculating the hazard from

gridded seismicity for the rest of California, we did not use the events extracted from the creeping section.

We lowered the magnitude of Parkfield characteristic earthquakes to 6.5. This is more similar to the magnitude observed for the 1922, 1934, and 1966 Parkfield earthquakes, than the M6.9 derived from using the area of this fault segment.

We also treated earthquakes on or near the Brawley Zone in southern California differently than other events. We removed events within 10 km of the “Brawley fault” used in the 1996 maps. The seismicity grid determined from these events was anisotropically smoothed with a 75 km correlation distance parallel to the strike of the Brawley zone and 10 km perpendicular to the zone.

Some of the faults segmented in the 1996 maps (e.g., the Maacama fault), were treated as unsegmented faults in the 2002 maps (see Petersen et al., 2000). Slip rates were revised for several faults, including the Sierra Madre and Raymond faults, based on recent findings. The Mount Diablo thrust (WGCEP, 2002) and Puente Hills and San Joaquin Hills blind thrusts were added to the hazard maps. The Compton thrust was removed because of lack of evidence of Quaternary offset. Again, details of the changes for California faults will be documented in a separate report by the California Geological Survey.

One of the problems with the California seismicity model used in the 1996 maps (and CA seismicity models published by others) was that it over predicted the rate of M6.5-7.0 earthquakes, compared to the observed seismicity since 1850 (Petersen et al., 2000). In contrast, the seismicity model used for the 2002 maps predicts seismicity rates quite similar to the observed rates (Figure 6). So, we have reduced the difference in our current model. The agreement between the predicted and observed seismicity rates is due to a number of factors, including 1) the 2/3 weight of characteristic model and 1/3 weight of GR model for fault recurrence, 2) the inclusion of aleatory and epistemic uncertainties for the Mchar of the faults, 3) the use of the new area-magnitude relations of Ellsworth and Hanks and Bakun (2002), and 4) avoiding magnitude overlap between the hazard calculations for the gridded seismicity and the faults (see below).

### Cascadia Subduction Zone

The probabilistic ground motion estimates for the coast of Oregon have significantly decreased. For the 2002 maps, we use multiple models for the geometry of the subduction zone determined. Figure 7 shows the landward edges of the rupture zone used for the draft maps, compared with that used for the 1996. One of the models is a modification of that used in the 1996 maps; the others are from thermal modeling of the subducted plate by Hyndman and Wang (1995) and Flück et al. (1997). The rupture model used in 1996 was a plane with a landward edge at 123.8°W longitude. While this model is similar to the base of the transition zone of Flück et al. (1997) in northern California and parts of western Washington, it is further inland along western Oregon than the base of the transition zone. The revised model basically follows the configuration of the eastern edge of the rupture zone used in the 1996 maps in northern California and Oregon and then doglegs to the northwest in northwestern Washington

state (Figure 7). This new model was assigned a weight of 0.5 in the hazard calculations. We maintained the depth of 20 km for the eastern edge of this zone that was used in the 1996 maps.

We also used three models based on the work of Flick et al. (1997). We gave 0.1 weight to a model where the landward edge of the rupture zone is the base of the elastic zone (furthest from the coast). We gave 0.2 weight to the model where the landward edge of the rupture zone is along the midpoints between the base of the elastic and transition zones. We assigned 0.2 weight to the model where the landward edge of the rupture zone is at the base of the transition zone. The higher weights for the midpoint and transition zone models were chosen because we thought it likely that seismic ruptures will propagate down dip from the zone that is totally locked in the interseismic period. Because the current models from Flick et al. (1997) have rupture zones farther offshore of Oregon than what was used in the 1996 maps, the hazard estimates decrease along the coast of Oregon.

Recent work by McCaffrey et al. (2000) finds a locked zone extending farther inland from modeling of GPS data, such that the 1996 eastern boundary is similar to the edge of the seaward locked zone that they report in their paper. We feel that the issue of the position and geometry of the locked zone is still in a state of flux. Ongoing modeling and continuing GPS measurements will reduce the uncertainty in the position of the eastern edge of the locked zone in the future.

Another factor that decreases the hazard estimates for Cascadia earthquakes is the weighting of the **M9.0** and **M8.3** scenarios. For 2002, we assigned a weight of 0.5 for each scenario, in keeping with comments at the Pacific Northwest workshop. For 1996, the weights were 0.67 for the **M8.3** scenario and 0.33 for the **M9.0** scenario. Since 1996, the **M9.0** scenario has gained credibility. The recurrence time for the **M9.0** scenario is about 500 years, longer than the recurrence time used for the **M8.3** scenario. Assigning higher weight to the **M9.0** scenario, therefore, results in lower probabilistic ground motions.

### Puget Lowland

Three newly characterized faults are used for the Puget Lowland area of Washington state: the Devil's Mountain fault, the Strawberry Point fault, and the Utsulady Point fault, based on the work of Johnson et al. (2001). The trace of the Seattle Fault has been revised since the 1996 maps. Now three traces are used (Johnson et al., 1999) instead of a single trace. We kept the recurrence parameters for the Seattle Fault the same as used in 1996: half weight to a characteristic model with a recurrence time of 5000 years and half weight to a Gutenberg-Richter (GR) model that predicts, on average, a  $M \geq 6.5$  earthquake every 1100 years. Only the northern trace of the fault was used for the characteristic model. The GR recurrence rates were divided evenly among the three traces. The GR rate is consistent with the rate of paleoearthquakes observed on the Toe Jam Hill fault on Bainbridge Island (Nelson et al., 1999). This fault is thought to be a back thrust of the Seattle fault zone. The characteristic magnitudes for the three traces (from south to north) were 7.2, 7.1, and 7.2, based on their lengths.

An areal source zone for the Puget Lowland (and part of the Georgia Strait region) is used in the 2002 maps (Figure 8). The Puget Lowland areal zone model is

given equal weight with the spatially-smoothed seismicity model. Both of these models are meant to account for the hazard on faults in the region that are either unknown or uncharacterized. We determined the  $a$ -value for the areal source zone from the observed rate of  $M \geq 5.0$  shallow earthquakes since 1928. The  $M_{\max}$  values used within the areal zone were adjusted so that there was no overlap with the magnitudes used in hazard calculation of the faults. We did apply a larger  $M_{\max}$  of 7.3 for the areal zone, which is larger than the  $M_{\max}$  of 7.0 used for the gridded seismicity when not over faults. By increasing this  $M_{\max}$  to 7.3, the areal zone accounts for 2.7 mm/yr of north-south contraction across the zone (assuming faults strike east-west, dip at 45 degrees, and with a 20 km seismogenic thickness), not including the slip rate on faults also used in the model (e.g., Seattle, S. Whidbey Island). Here we used the formula relating convergence (or extension) rate  $v$  to the seismic moment rate for a volume, such that  $v = (\text{Moment rate}) / (2 \mu L h)$ . In this formula,  $\mu$  is the shear modulus,  $L$  is the average dimension of the zone perpendicular to the convergence direction, and  $h$  is the seismogenic thickness. This formula for dipping faults was developed by Anderson (1979) and Hyndman et al. (2001) and is a specific application of that in Kostrov (1974). Combined with the slip rates of the known faults, the areal zone gives a north-south contraction rate consistent with the approximately 3-5 mm/yr observed with GPS data (Miller et al., 2001; Mazotti et al., 2002). The inclusion of the model with the areal zone has a small but significant effect on the seismic hazard maps. It tends to increase the probabilistic ground motions (2% PE in 50 years) near the edges of the areal zone by about 5-10%, compared to the ground motions calculated just from the gridded seismicity.

### Deep Earthquakes

The seismicity parameters used for the deep intraslab earthquakes (depth > 35 km) were also revised for the 2002 maps. For the Puget Lowland region, we now use the  $b$ -value determined by the maximum likelihood method from deep earthquakes only in the Puget Lowland region (including the Georgia Strait region). This maximum likelihood  $b$ -value of 0.4 found from the Puget Lowland deep events was significantly lower than that determined using all the deep events including northern California deep earthquakes. We could not determine a well-constrained  $b$ -value for the deep northern California events, since the largest event was  $M_{5.4}$  and we use a minimum magnitude of 4.0. We therefore assumed a  $b$ -value of 0.8 for these events, consistent with that used for the shallow events. It is clear that the frequency-magnitude behavior of deep Puget Lowland events differs from that of deep northern California events. There have been deep events greater than or equal to  $M_{6.5}$  in the Puget Sound region in 1949, 1965, and 2001. We decreased the  $M_{\max}$  used in the hazard calculation for the deep events to 7.2, for the 2002 maps. Most catalogs list the moment magnitude of the 1949 event as 7.1, although this has been revised downward to 6.9 in the catalog from the Canadian Geological Survey (G. Rogers, written comm., 2000). We chose an  $M_{\max}$  of 7.2 just above the generally-quoted magnitude of the 1949 event.

## Basin and Range

Slip rates for WUS faults were re-evaluated and many were altered from 1996. The basic inputs were from the USGS Quaternary Fault and Fold database. These changes will be documented in separate texts. In many cases, more accurate fault traces were available for the 2002 maps, based on the traces used for the USGS Quaternary Fault Database. No changes were made in the shear zones in western Nevada and eastern California used in the 1996 maps.

The recurrence rates and characteristic magnitudes of the segments of the Wasatch Fault were very similar to those used in 1996. Because we are now using the Wells and Coppersmith (1994) magnitude-length relations for “all” fault types, some of the characteristic magnitudes along the Wasatch Fault have decreased by 0.1 magnitude unit compared to the 1996 maps, which used the magnitude-length relation for normal faulting (see above). We used the McCalpin and Nishenko (1996) mean rates of occurrence for each segment, based on trenching results.

We gave a weight of 20% to a truncated Gutenberg-Richter model for the segments of the Wasatch Fault, where the  $a$ -value for each segment is determined from its geologic slip rate. Using a purely characteristic model could underestimate the recurrence of M6.5 earthquakes along the fault. While the gridded seismicity calculation does take into account earthquakes from magnitude 5.0 up to magnitude 7.0 (or the characteristic magnitude of each segment if it is lower than M7.0), it may underestimate the occurrence of events around M6.5. Earthquakes with magnitudes near 6.5 may not have surface rupture and their displacements may not be observable in trenches dug across the fault. The 20% weight represents a middle ground of the weights supported by the experts we queried (G. Christenson, J. Pechmann, R.B. Smith, W. Arabasz, D. Schwartz, J. Kimball). This 20% weight predicts a recurrence time of about 150 years for  $M \geq 6.5$  earthquakes on the Wasatch fault, when the gridded seismicity and paleoseismic recurrence rates are also considered. Given the short historical record of about 150 years, this recurrence time cannot be ruled out. The weighting of the GR model for the Wasatch fault needs to be further examined. Using higher weights for the GR model will give higher values of probabilistic ground motions, because of the more frequent occurrence of M6.5 earthquakes, compared with M7 earthquakes that rupture entire fault segments.

We did some tests on the effect of multiple-segment rupture models on the hazard calculated from the Wasatch Fault, as proposed by R.B. Smith (written communication 2001; Chang and Smith, 2002). Our initial tests found that assuming every other large earthquake on the Provo segment also ruptured the Salt Lake City segment did not have a major effect on the hazard maps for 2% probability of exceedance in 50 years. It is difficult to characterize the recurrence rate and rupture zones for multiple-segment scenarios from the dating of paleoearthquakes at limited locations along the Wasatch fault. However, we intend to look at this multiple-segment rupture model on the Wasatch fault more fully in the future.

A logic tree of  $M_{char}$  was applied for each segment of the Wasatch fault, for the characteristic model. The logic tree was  $M_{char} - 0.2$  m.u.,  $M_{char}$ , and  $M_{char} + 0.2$  m.u., with a weighting of 0.2, 0.6, 0.2. The mean recurrence rate was used for each branch. This logic tree had virtually no effect on the mean hazard curve compared to a model using only  $M_{char}$ .

An areal zone for the  $M_{max}$  used for the gridded seismicity hazard calculation was added for the central Nevada Seismic Zone (CNSZ) for the 2002 maps (Figure 9), to increase the  $M_{max}$ . This was done to accommodate the approximately 2 mm/yr of extension that is observed across this area during recent campaign GPS studies (Thatcher et al., 1999; Wernicke et al., 2000). The long-term slip rates of faults in this area are a small fraction of the extension rate observed with GPS. By increasing the  $M_{max}$  used in the hazard calculation to 7.5 for the gridded seismicity (compared to the typical  $M_{max}$  of 7.0), the gridded seismicity rate now accounts for about 1 mm/yr of extension (using the formula above relating deformation rate to seismic moment rate), assuming the faults are aligned perpendicular to the extension direction. Adding in the long-term slip rates from the faults used in the hazard maps yields an extension rate similar to that observed from GPS. Using the new  $M_{max}$  zone makes about a 10% increase in the probabilistic ground motions at 2% PE in 50 years. This procedure addresses the concern that, given the spate of large earthquakes in this zone during the 20<sup>th</sup> century, the long recurrence times derived for the faults using their long-term slip rates may underestimate the hazard there.

### Changes in Background Zones

There was one change to the background zones used in 1996 (see Figure 10). The eastern Snake River Plain zone was reduced in size based on the suggestion of S.J. Payne, R.P. Smith, and J. Zollweg. This zone represents an area of relative seismic quiescence, high heat flow, and anomalous crustal and upper mantle structure (S.J. Payne and R.P. Smith, written communication, 2001). The western end of this background zone was moved to the east, recognizing that active faults have been found in the western portion of the zone used for 1996.

### Fixing overlap of magnitudes between gridded seismicity and faults

One problem with our methodology of combining hazard from the gridded seismicity and faults is the potential overlap of magnitude. Although this overlap has only a very minor effect on the hazard estimates, we fixed this problem for the 2002 maps. Now the  $M_{max}$  for the gridded seismicity calculation is lowered over dipping faults and within 10 km of vertical faults so that there is no magnitude overlap. For the GR case the  $M_{max}$  of the gridded seismicity calculation is set to  $M_{6.5}$ , which is the  $M_{min}$  of the GR relation for the fault. For the characteristic case, the  $M_{max}$  is set to  $M_{char}$  or  $M_{7.0}$ , whichever is smaller.  $M_{max}$  is set to 7.0 for the gridded seismicity calculation for areas off of faults. When the hazard is calculated from the gridded seismicity, two runs are performed using the  $M_{max}$  grids for the characteristic and GR

fault cases. The hazard curves from these two runs are then added with the appropriate weight for the characteristic and GR models used for faults in that area.

### WUS Attenuation Relations

One of the major changes in 2002 was our division of the WUS into an area of extensional tectonics and an area with non-extensional tectonics, for the purpose of using different sets of attenuation relations. This was necessitated by the addition of the Spudich et al. (1999) attenuation relation, which is appropriate for areas of extensional tectonics. Figure 4 shows the faults used in the 2002 maps, color coded by whether they are in the extensional or non-extensional areas we have delineated. For faults within the extensional area, we use the following attenuation relations, all with equal weight: Boore et al., (1997), Sadigh et al. (1997), Abrahamson and Silva (1997), Spudich et al., 1999, and Campbell and Bozorgnia (2003). For faults outside of the extensional area, we exclude the Spudich et al. (1999) relation and give the other four relations 0.25 weight. We only used the hanging wall terms in Abrahamson and Silva (1997) and Campbell and Bozorgnia (2003) for thrust or reverse faults.

The hazard calculations for gridded seismicity were also divided into extensional and non-extensional zones. The same set of attenuation relations and weights were used for the gridded seismicity hazard calculation as for the faults. For the gridded seismicity calculation in non-extensional areas, we assumed a random fault type. Thus we used half of the logarithmic term for thrust faults specified in Sadigh et al. (1997) and Abrahamson and Silva (1997). For Campbell and Bozorgnia (2003), we used 0.25 times the sum of the thrust and reverse terms. For Boore et al. (1997) we used the average of the strike slip and thrust terms. The gridded seismicity hazard calculation for extensional areas used attenuation relations for strike slip faulting.

One important question is how attenuation relations for “rock” sites should be adjusted to the B-C boundary site condition ( $V_{s30} = 760$  m/s) used in the national seismic hazard maps. The external review panel advised us to formally ask the principal author of each attenuation relation to get their recommendation on how to adjust their values, if at all. Norm Abrahamson (Abrahamson and Silva, 1997), Bob Youngs (representing Sadigh et al., 1997), and Paul Spudich (Spudich et al., 1999) all recommended that we do not adjust their “rock” attenuation values for the B-C boundary site condition. The primary justification for this approach was that the  $V_{s30}$  values have not been measured for most of the sites used to develop the attenuation relations. Ken Campbell recommended using an average of the natural log terms for the firm and soft rock site conditions from Campbell and Bozorgnia (2003) and then adjusting from  $V_{s30} 620$  m/s to  $V_{s30} 760$  m/s using the Boore et al. (1997) factors. We followed the recommendations of each of these authors for their respective attenuation relation.

At the ATC workshop, it was suggested that we account for the effect of rupture directivity in the hazard calculations by increasing the standard deviation ( $\sigma$ ) of the ground motion distribution for sites near a fault. We did not implement this increase for the 2002 maps, since it was unclear how much to increase the near-source  $\sigma$ . This is not in the published literature. We will seek out advice on what increases in  $\sigma$

should be used for 1 Hz and lower frequencies from researchers who have quantified the effects of rupture directivity, for future maps.

An important change in the 2002 maps compared to the 1996 maps is the inclusion of the Sadigh et al. (1997) attenuation relations for the M9.0 Cascadia subduction-zone earthquake scenario. Previously, we only used Youngs et al. (1997) for the M9.0 earthquakes, because the Sadigh et al. (1997) equations did not work for  $M > 8.5$  (there is a term with  $[8.5 - M]$  to the 2.5 power). For the M9.0 scenario in the 2002 maps, we assigned half weight to the Youngs et al. (1997) attenuation relation for M9.0 and half weight to the Sadigh et al. (1997) relation using M8.5, for distances less than 60 km. This equal weighting scheme was used for distances where the Sadigh et al. (1997) PGA values for M8.5 exceeded those of Youngs et al. (1997) for M9.0. For larger distances ( $R > 60$  km), where the Youngs et al. (1997) PGA values were the higher of the two, we only used the Youngs et al. (1997) relations. This weighting scheme follows that used by Geomatrix Consultants (1995) and is a more consistent treatment for the M8.3 and M9.0 earthquakes.

For the M8.3 scenario, we give equal weight to the Youngs et al. (1997) interface earthquake relation and the Sadigh et al. (1997) crustal earthquake attenuation for distances up to 70 km. For larger distances we gave full weight to Youngs et al. (1997). For distances less than 70 km, the PGA values predicted by Sadigh et al. are higher than those from Youngs et al. (1997). Beyond 70 km, the PGA is larger for the Youngs et al. (1997) relation for M8.3 than for the Sadigh et al. (1997) relation. For both the M8.3 and M9.0 scenarios, we apply the change in weighting with a 30 km wide taper centered on the aforementioned distances. In the 1996 maps, we gave equal weight to both relations for the M8.3 scenario, for all distances.

The rationale for including the Sadigh et al. (1997) relations derived from crustal earthquakes for computing the hazard from great subduction-zone events is that at close distances the limited database of observed close-in ground-motion values for great subduction-zone earthquakes may cause an underestimation of the typical ground motions for M8-9 earthquakes (Geomatrix Consultants, 1995; Gregor et al., 2002). The empirical data at large magnitudes and close distances used by Youngs et al. (1997) are dominated by the 1985 M8 Michoacan, Mexico and the 1985 M7.9 Valparaiso, Chile earthquakes, which had relatively low peak ground acceleration (PGA) values near the coast (see Geomatrix Consultants, 1995). In contrast, the relatively high peak accelerations observed for the 1992 M7.1 Petrolia, California earthquake, which may have occurred on the Cascadia subduction zone, are similar to those expected for crustal earthquakes (Geomatrix Consultants, 1995). Finite-fault simulations by Gregor et al. (2002) also imply larger ground motions for great subduction-zone earthquakes compared to the Youngs et al. (1997) empirical relations. We considered using the new subduction-zone attenuation relations determined by Gregor et al. (2002) from finite-fault simulations. We think that these new attenuation relations need to be further evaluated by the seismological community before they are included in the national seismic hazard maps.

The inclusion of the Sadigh et al. (1997) attenuation relations in the M9.0 scenario significantly increases the probabilistic ground motions along the Oregon and Washington coasts compared to just using the Youngs et al. (1997) relations. However, the probabilistic ground motions along the Oregon coast in the 2002 maps are still

lower than those in the 1996 maps (reduced by about 10-15% for PGA, 1 Hz, and 5 Hz spectral accelerations at 2% PE in 50 years), because of the other configurations used for the eastern edge of the rupture zone of Cascadia earthquakes and the increased weighting for the M9.0 scenario (see below).

We essentially used three attenuation relations for the deep earthquakes (depth > 35 km). The first was the Youngs et al. (1997) relation for intraslab events. The second and third are from Atkinson and Boore (2002) rock-site relations for intraslab earthquakes. Atkinson and Boore (2002) give relations from a regression on global data and corrections for use with earthquakes in the Cascadia region. Based on guidance from G.M. Atkinson (written comm., 2002), we gave each of these approaches equal weight. So the weighting scheme was: Youngs et al. (1997) 0.5 weight, Atkinson and Boore (2002) global relation 0.25 weight, and Atkinson and Boore (2002) Cascadia region relation 0.25 weight. The Atkinson and Boore (2002) relations were evaluated for a BC site condition by taking the log average of the predicted ground motions for site classes B and C, as recommended by G.M. Atkinson (written comm., 2002). Studies of the 2001 Nisqually earthquake demonstrated that the Atkinson and Boore (2000) global relation did a better job of predicting the observed spectral accelerations at 1 Hz and 5 Hz than did Youngs et al. (1997), especially at hypocentral distances greater than 100 km.

For all western U.S. hazard calculations, we truncated the ground-motion distribution at three standard deviations.

### **Acknowledgments**

William Bryant and Tianqing Cao of the California Geological Survey assembled the fault database for California and provided essential guidance on California issues. We thank all of the people who provided comments on the draft maps and who participated in the regional workshops. We particularly thank the external review panel of Allin Cornell, Robert Herrmann, Jeffrey Kimball, Michael Reichle, and Robert Smith for their critical comments and advice. Craig Weaver, David Schwartz, Buddy Schweig, David Boore, Tom Hanks, and John Filson provided helpful advice and support. We thank Nancy Dickman for her efforts at placing the draft maps and documentation on our website.

### **References**

- Abrahamson, N.A. and W.J. Silva (1997). Empirical response spectral attenuation relations for shallow crustal earthquakes, *Seis. Res. Letts.*, v. 68, no. 1, pp. 94-127.
- Anderson, J.G. (1979). Estimating the seismicity from geologic structure for seismic risk studies, *Bull. Seism. Soc. Am.*, v. 69, pp. 205-214.
- Atkinson, G.M. and D.M. Boore (2002). Empirical ground-motion relations for subduction zone earthquakes and their application to Cascadia and other regions, in review.

- Atkinson, G.M. and D. M. Boore (1995). Ground motion relations for eastern North America, *Bull. Seism. Soc. Am.*, v. 85, pp. 17-30.
- Bakun, W.H. and M.G. Hopper (2002). The 1811-12 New Madrid, Missouri, and the 1886 Charleston, South Carolina, earthquakes, in review.
- Bakun and McGarr (2002). Earthquake shaking in different stable continental regions--one attenuation model doesn't fit all, submitted to *Geophys. Res. Letts.*
- Bendick, R., R. Bilham, E. Fielding, V. K. Gaur, S.E. Hough, G. Kier, M.N. Kulkarni, S. Martin, K. Mueller, and M. Mukul (2001). The 26 January 2001 "Republic Day" earthquake, India, *Seism. Res. Letts.*, v. 72, no. 3, pp. 328-335.
- Boore, D.M. and G.M. Atkinson (1987). Stochastic prediction of ground motion and spectral response parameters at hard-rock sites in eastern North America, *Bull. Seism. Soc. Am.*, v. 77, pp. 440-467.
- Boore, D.M., W.B. Joyner, and T.E. Fumal (1997). Equations for estimating horizontal response spectra and peak acceleration from western North American earthquakes: a summary of recent work, *Seism. Res. Letts.*, v. 68, pp. 128-153.
- Campbell, K.W. (2002). Prediction of strong ground motion using the hybrid empirical method: example application to eastern North America, submitted to *Bull. Seism. Soc. Am.*
- Campbell, K.W. and Y. Bozorgnia (2003). Updated near-source ground motion (attenuation) relations for the horizontal and vertical components of peak ground acceleration and acceleration response spectra, *Bull. Seism. Soc. Am.*, in press.
- Chang, W.L. and Smith, R.B. (2002). Integrated seismic hazard analysis of the Wasatch Front, Utah, *Bull. Seism. Soc. Am.*, v. 92, pp. 1904-1922.
- Cramer, C.H. (2001). A seismic hazard uncertainty analysis for the New Madrid seismic zone, *Engineering Geology*, 62, pp. 251-266.
- Flück, P., R.D. Hyndman, and K. Wang (1997). Three-dimensional dislocation model for great earthquakes of the Cascadia subduction zone, *J. Geophys. Res.*, 102, pp. 20,539-20,550.
- Frankel, A. (1995). Mapping seismic hazard in the Central and Eastern United States, *Seism. Res. Letts.*, v. 66, no. 4, pp. 8-21.
- Frankel, A., C. Mueller, T. Barnhard, D. Perkins, E. Leyendecker, N. Dickman, S. Hanson, and M. Hopper (1996). National seismic-hazard maps: documentation June 1996, *U.S. Geological Survey, Open-file Report 96-532*, 110 pp.
- Frankel, A., C. Mueller, S. Harmsen, R. Wesson, E. Leyendecker, F. Klein, T. Barnhard, D. Perkins, N. Dickman, S. Hanson, and M. Hopper (2000) USGS National Seismic Hazard Maps, *Earthquake Spectra*, v. 16, pp. 1-19.
- Geomatrix Consultants (1995). Seismic design mapping state of Oregon, Final Report, prepared for the Oregon Department of Transportation, Salem, Oregon.
- Gregor, N.J., W.J. Silva, I.G. Wong, and R.R. Youngs (2002). Ground-motion attenuation relationships for Cascadia subduction zone megathrust earthquakes based on a stochastic finite-fault model, *Bull. Seism. Soc. Am.*, v. 92, pp.1923-1932.
- Hanks, T.C. and W.H. Bakun (2002). A bilinear source-scaling model for  $M - \log A$  observations of continental earthquakes, *Bull. Seism. Soc. Am.*, v. 92, pp. 1841-1846.

- Hough, S.E., J.G. Armbruster, L. Seeber, and J.F. Hough (2000). On the Modified Mercalli intensities and magnitudes of the 1811-12 New Madrid earthquakes, *J. Geophys. Res.*, v. 105, pp. 23,839-23,864.
- Hyndman, R.D. and K. Wang (1995). The rupture zone of Cascadia great earthquakes from current deformation and the thermal regime, *J. Geophys. Res.*, v. 100, pp. 22,133-22,154.
- Hyndman, R.D., S. Mazzotti, D. Weichert, and G.C. Rogers (2001). Frequency of large crustal earthquakes in Puget Sound- S. Georgia Strait predicted from geodetic and geological deformation rates, submitted to *J. Geophys. Res.*
- Johnson, S.Y., S.V. Dadisman, J.R. Childs, and W.D. Stanley (1999). Active tectonics of the Seattle fault and central Puget Sound, Washington—implications for earthquake hazards, *Geol. Soc. Am. Bull.*, v. 111, pp. 1042-1053.
- Johnson, S.Y., S.V. Dadisman, D.C. Mosher, R.J. Blakely, and J.R. Childs (2001). Active tectonics of the Devils Mountain fault and related structures, northern Puget Lowland and eastern Strait of Juan de Fuca region, Pacific Northwest, *U.S. Geological Survey Professional Paper 1643*, 46 pp., 2 plates.
- Johnston, A.C. (1996a). Seismic moment assessment of stable continental earthquake, III., 1811-182 New Madrid, 1886 Charleston, and 1755 Lisbon, *Geophys. J. Int.*, v. 126, pp. 314-344.
- Johnston, A.C. (1996b). Seismic moment assessment of earthquakes in stable continental regions—I. Instrumental seismicity, *Geophys. J. Int.*, v. 124, pp. 381-414.
- Johnston, A.C., K.J. Coppersmith, L.R. Kanter, and C.A. Cornell (1994). The earthquakes of stable continental regions: assessment of large earthquake potential, EPRI TR-102261, J.F. Schneider, ed., Electric Power Research Institute, 309 pp.
- Kostrov, V.V. (1974). Seismic moment and energy of earthquakes, *Izv. Acad. Sci. USSR, Phys. Solid Earth*, v. 1, pp. 23-44.
- Mazzotti, S., H. Dragert, R.D. Hyndman, M.M. Miller, and J.A. Henton, (2002). N-S shortening in the Puget-Georgia basin estimated by GPS, submitted to *EPSL*.
- McCaffrey, R., M.D. Long, C. Goldfinger, P.C. Zwick, J.L. Nabelek, C.K. Johnson, and C. Smith (2000). Rotation and plate locking at the southern Cascadia subduction zone, *Geophys. Res. Letts.*, 27, pp. 3117-3120.
- McCalpin, J.P. and S.P. Nishenko (1996). Holocene paleoseismicity, temporal clustering, and probabilities of future large ( $M > 7$ ) earthquakes on the Wasatch fault zone, Utah, *J. Geophys. Res.*, v. 101, pp. 6233-6253.
- Miller, M.M., D.J. Johnson, C.M. Rubin, H. Dragert, K. Wang, A. Qamar, and C. Goldfinger (2001). GPS-determination of along-strike variation in Cascadia margin kinematics: implications for relative plate motion, subduction zone coupling, and permanent deformation, *Tectonics*, v. 20, pp. 161-176.
- Nelson, A.R., S.K. Pezzopane, R.C. Bucknam, R. Koehler, C. Narwold, H.M. Kelsey, W.T. LaPrade, R.E. Wells, and S.Y. Johnson (1999). Late Holocene surface faulting in the Seattle fault zone on Bainbridge Island, Washington, *Seism. Res. Letts.*, v. 70, p.233.
- Petersen, M.D., W.A. Bryant, C.H. Cramer, T. Cao, N.S. Reichle, A.D. Frankel, J.J. Lienkaemper, P.A. McCrory, and D.P. Schwartz (1996). Probabilistic seismic

- hazard assessment for the state of California, *California Division of Mines and Geology Open-File Report 96-08*, U.S. Geological Survey Open-File Report 96-706.
- Petersen, M. D., C.H. Cramer, M.S. Reichle, A.D. Frankel, and T.C. Hanks (2000). Discrepancy between earthquake rates implied by historic earthquakes and a consensus geologic source model for California, *Bull. Seism. Soc. Am.*, v. 90, pp. 1117-1132.
- Sadigh, K., C.Y. Chang, J. Egan, F. Makdisi, and R. Youngs (1997). Attenuation relationships for shallow crustal earthquakes based on California strong motion data, *Seism. Res. Letts.*, v. 68, pp. 180-189.
- Somerville, P., N. Collins, N. Abrahamson, R. Graves, and C. Saikia (2001). Ground motion attenuation relations for the central and eastern United States, final report to U.S. Geological Survey.
- Spence, W., C.J. Langer, and G.L. Choy (1996). Rare, large earthquakes at the Laramide deformation front—Colorado (1882) and Wyoming (1984). *Bull. Seism. Soc. Am.*, v. 86, pp. 1804-1819.
- Spudich, P., W.B. Joyner, A.G. Lindh, D.M. Boore, B.M. Margaris, and J.B. Fletcher (1999). SEA99: A revised ground motion prediction relation for use in extensional tectonic regimes, *Bull. Seism. Soc. Am.*, v. 89, pp. 1156-1170.
- Street, R., G.A. Bollinger, and E. Woolery, (2002). Blasting and other mining-related activities in Kentucky -- A source of earthquake misidentification: *Seism. Res. Letts.*, v. 73, no. 5, pp. 739-750.
- Talwani, P. and W.T. Schaeffer (2001). Recurrence rates of large earthquakes in the South Carolina coastal plain based on paleoliquefaction data, *J. Geophys. Res.*, v. 106, pp. 6621-6642.
- Thatcher, W., G.R. Foulger, B.R. Julian, B.R., J. Svarc, E. Quilty, and G.W. Bawden, (1999). Present-day deformation across the Basin and Range province, western United States, *Science*, v. 283, pp. 1714-1718.
- Toro, G., N. Abrahamson, and J. Schneider (1997). Model of strong ground motions from earthquakes in the central and eastern North America: best estimates and uncertainties, *Seism. Res. Letts.*, v. 68, pp. 41-57.
- Tuttle, M.P. and E.S. Schweig (2000). Earthquake potential of the New Madrid seismic zone (abstract), *EOS, Trans. Am. Geophys. U.*, v. 81, S308-309.
- Wells, D.L. and K.J. Coppersmith (1994). New empirical relationships among magnitude, rupture length, rupture width, and surface displacements, *Bull. Seism. Soc. Am.*, v. 84, pp. 974-1002.
- Wernicke, B., A.M. Friedrich, N.A. Niemi, and R.A. Bennett (2000). Dynamics of plate boundary fault systems from Basin and Range Geodetic Network (BARGEN) and geologic data, *GSA Today*, 10, no. 11, pp. 1-7.
- Wheeler, R.L. and D.M. Perkins (2000). Research, methodology, and applications of probabilistic seismic-hazard mapping of the central and eastern United States—minutes of a workshop on June 13-14, 2000 at St. Louis University, U.S. Geological Survey, *Open-File Report 00-0390*, 18 pp.
- Wheeler, R.L. and C.H. Cramer (2002). Updated seismic hazard in the southern Illinois basin: geological and geophysical foundations for the 2002 USGS national seismic-hazard maps, *Seism. Res. Letts.*, v. 73, no. 5, pp. 776-791.

- Working Group on California Earthquake Probabilities (1995). Seismic hazards in southern California: probable earthquakes, 1994-2024, *Bull. Seism. Soc. Am.*, v. 85, pp. 379-439.
- Working Group on California Earthquake Probabilities (2002). Earthquake probabilities in the San Francisco Bay region: 2002-2031—*U.S. Geological Survey Circular 1189*, in review.
- Youngs, R. and K. Coppersmith (1985). Implications of fault slip rates and earthquake recurrence models to probabilistic hazard estimates, *Bull. Seism. Soc. Am.*, v. 75, pp. 939-964.
- Youngs, R.R., S.J. Chiou, W.J. Silva, and J.R. Humphrey (1997). Strong ground motion attenuation relationships for subduction zone earthquakes, *Seism. Res. Letts.*, v. 68, no. 1, pp. 58-73.

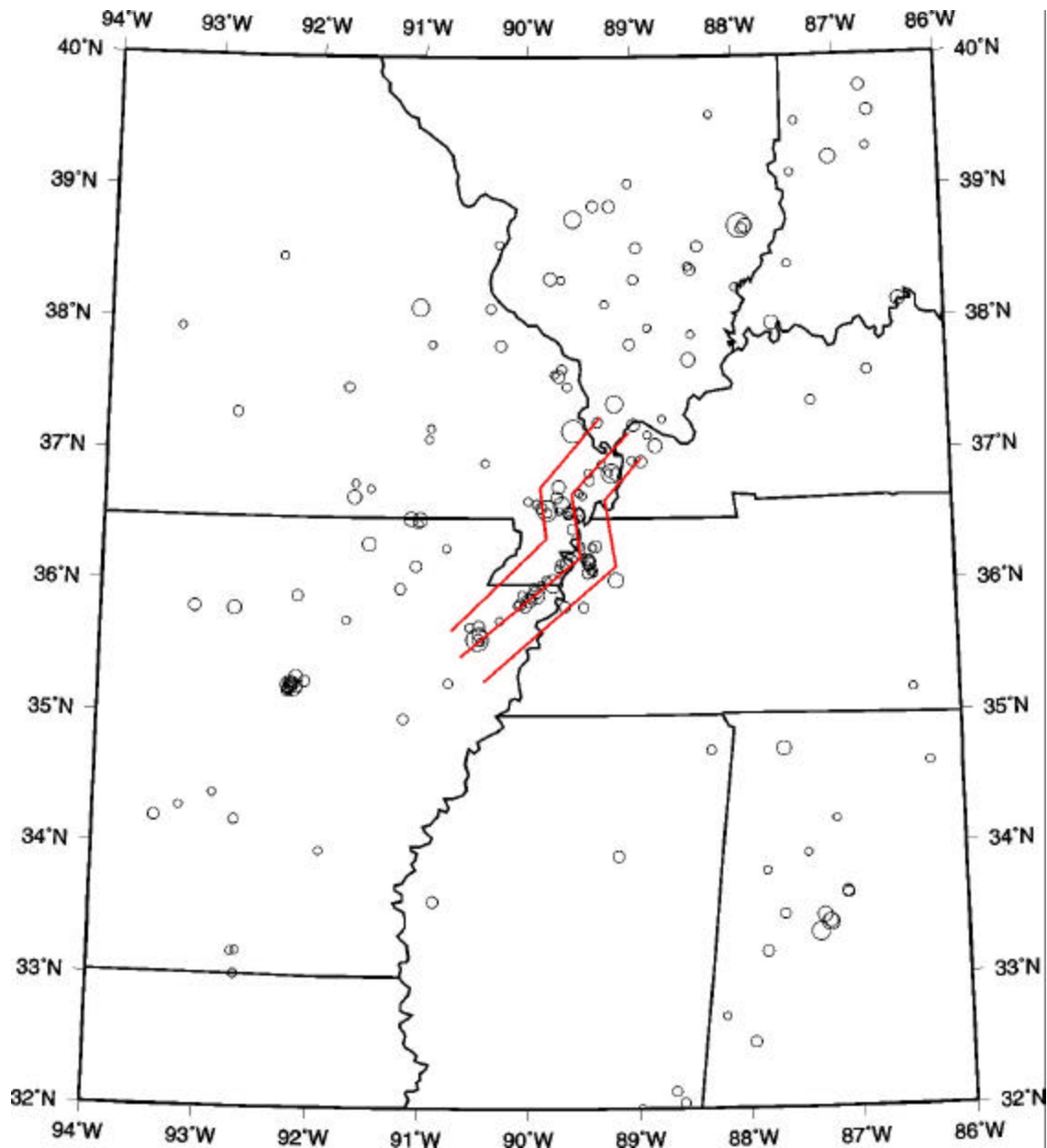


Figure 1. Fictitious faults (red) used to characterize the uncertainty in source location for New Madrid characteristic earthquakes. Circles are earthquakes with  $mblg \geq 3.0$  since 1976.

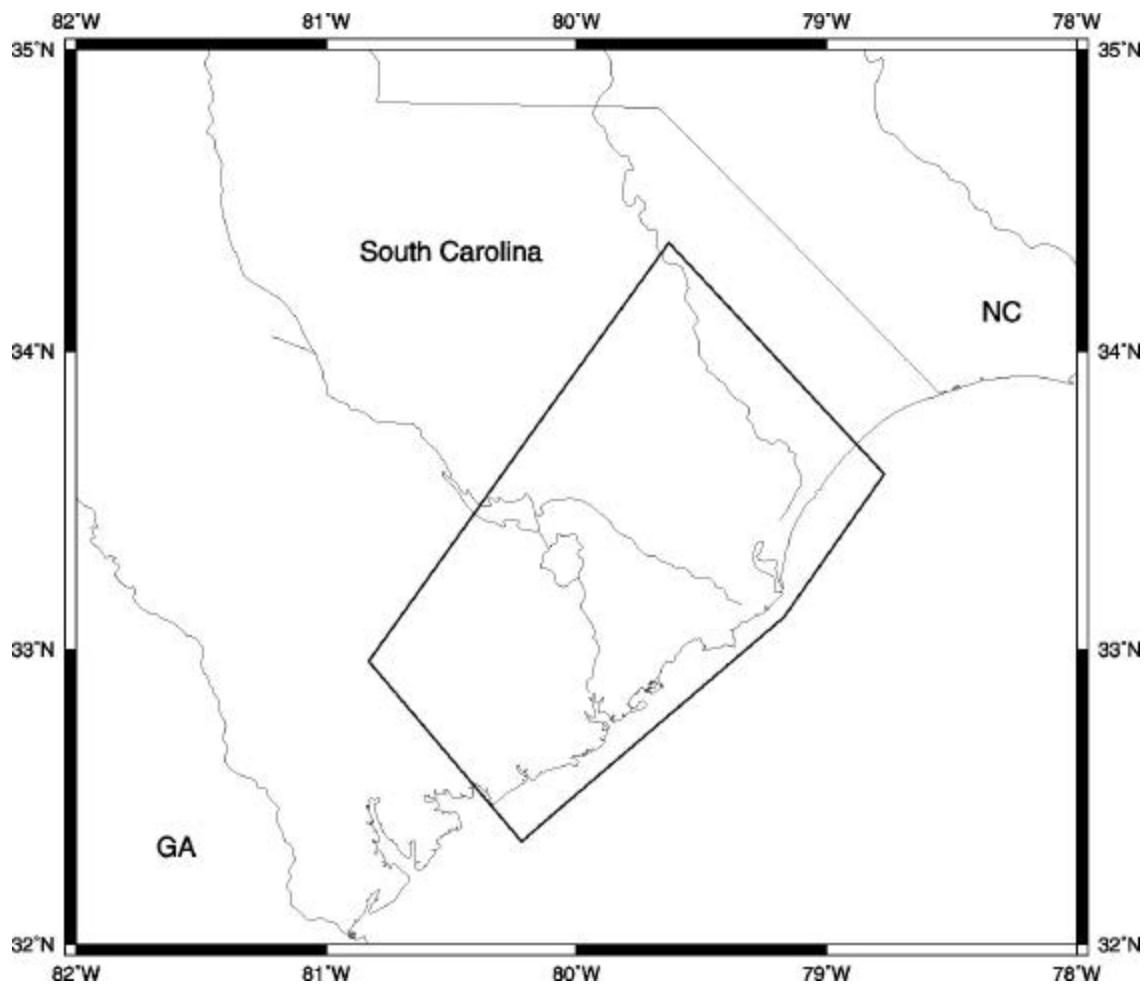


Figure 2. Broad areal source zone used for characteristic Charleston earthquakes. This model was given  $\frac{1}{2}$  weight.

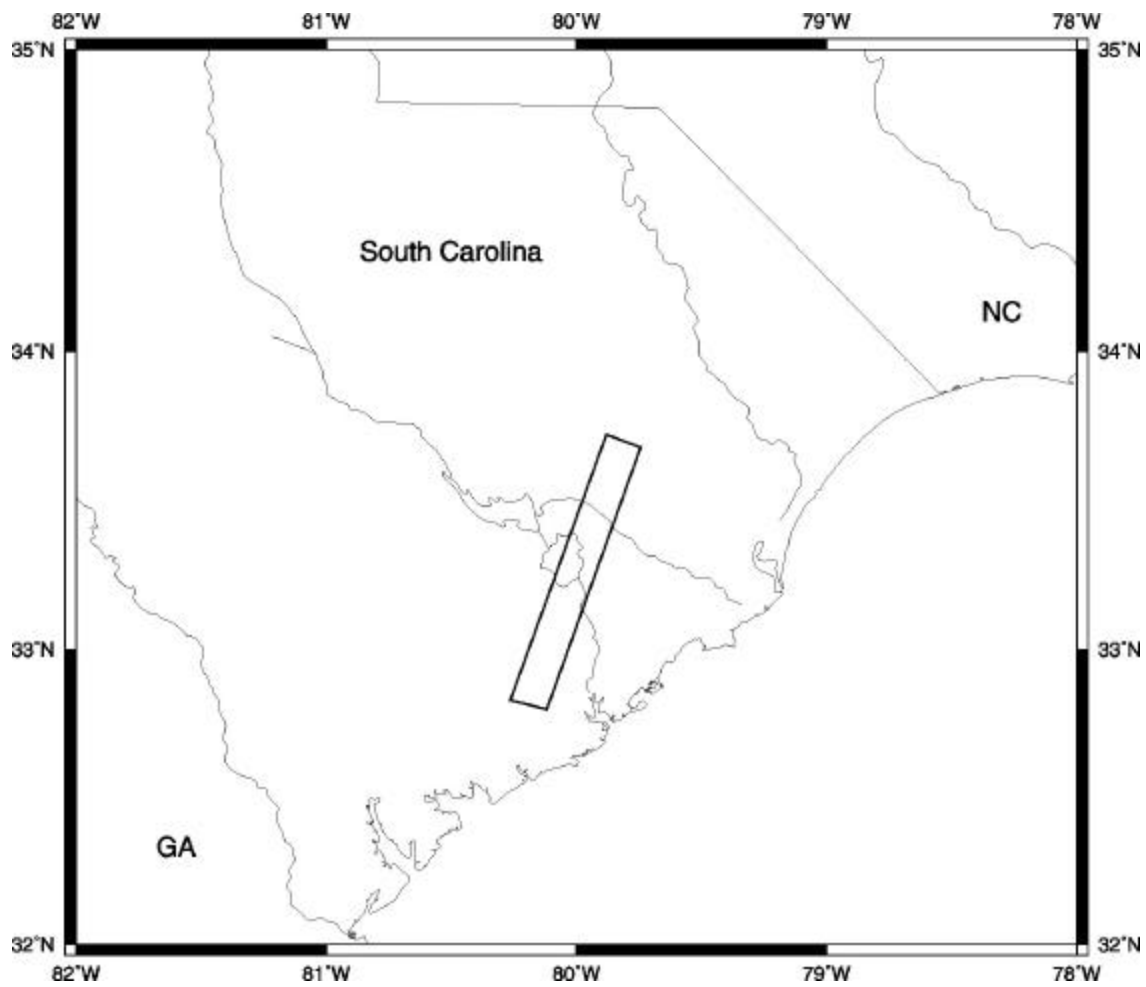


Figure 3. Narrow areal source zone used for characteristic Charleston earthquakes. This model was given  $\frac{1}{2}$  weight.

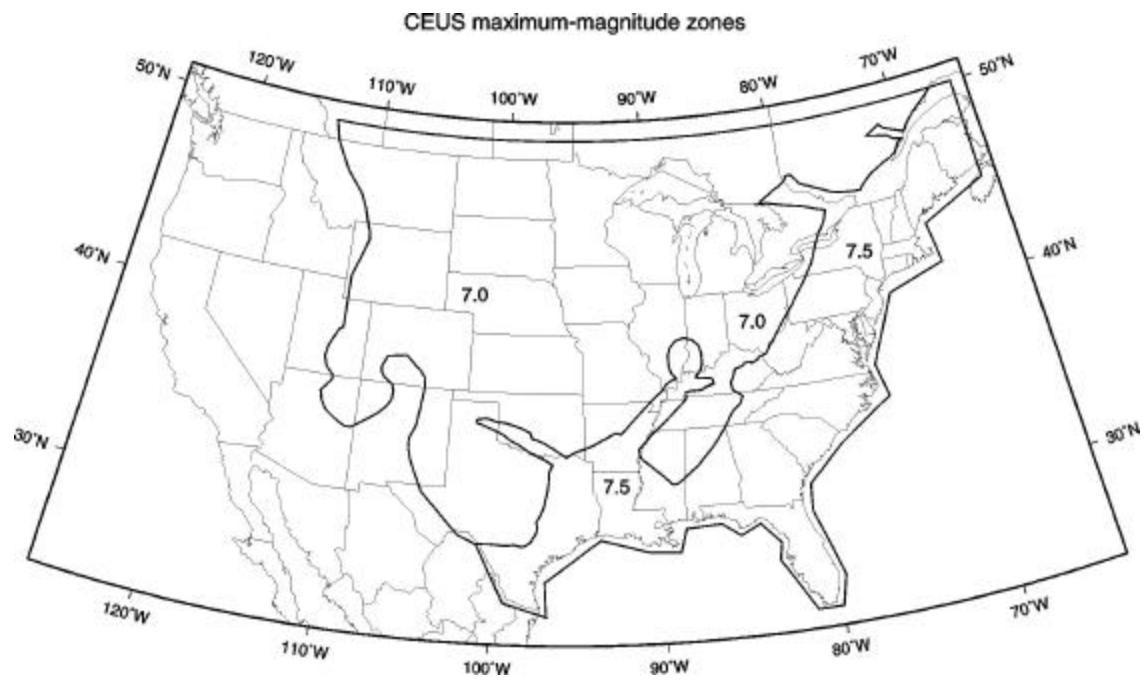


Figure 4. Maximum magnitude zones used for the Central and Eastern U.S.

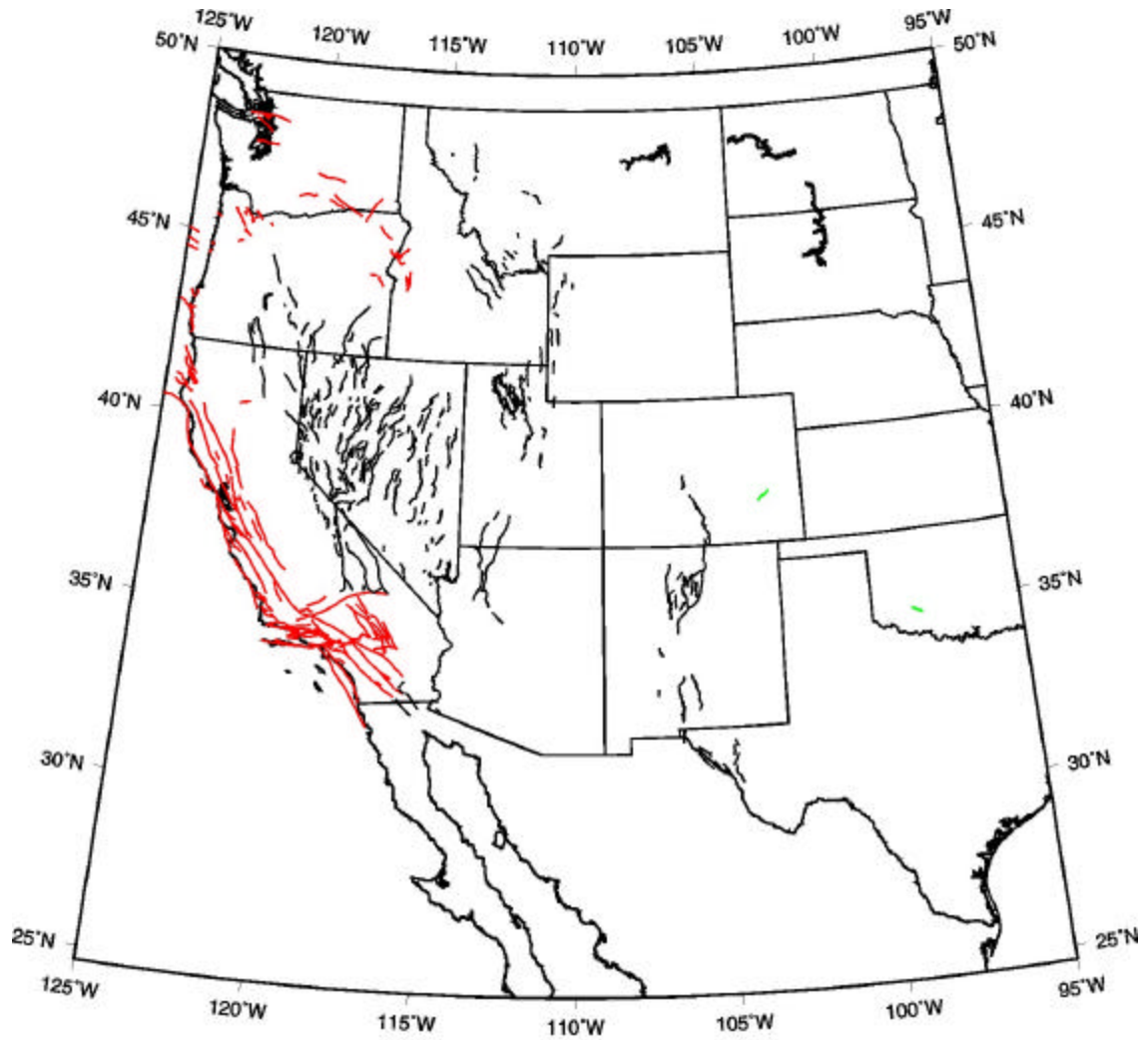


Figure 5. Faults used in 2002 maps. Red traces are faults in the non-extensional attenuation zone; black traces are faults in the extensional attenuation zone; green traces are faults in the Central and Eastern U.S. attenuation zone.

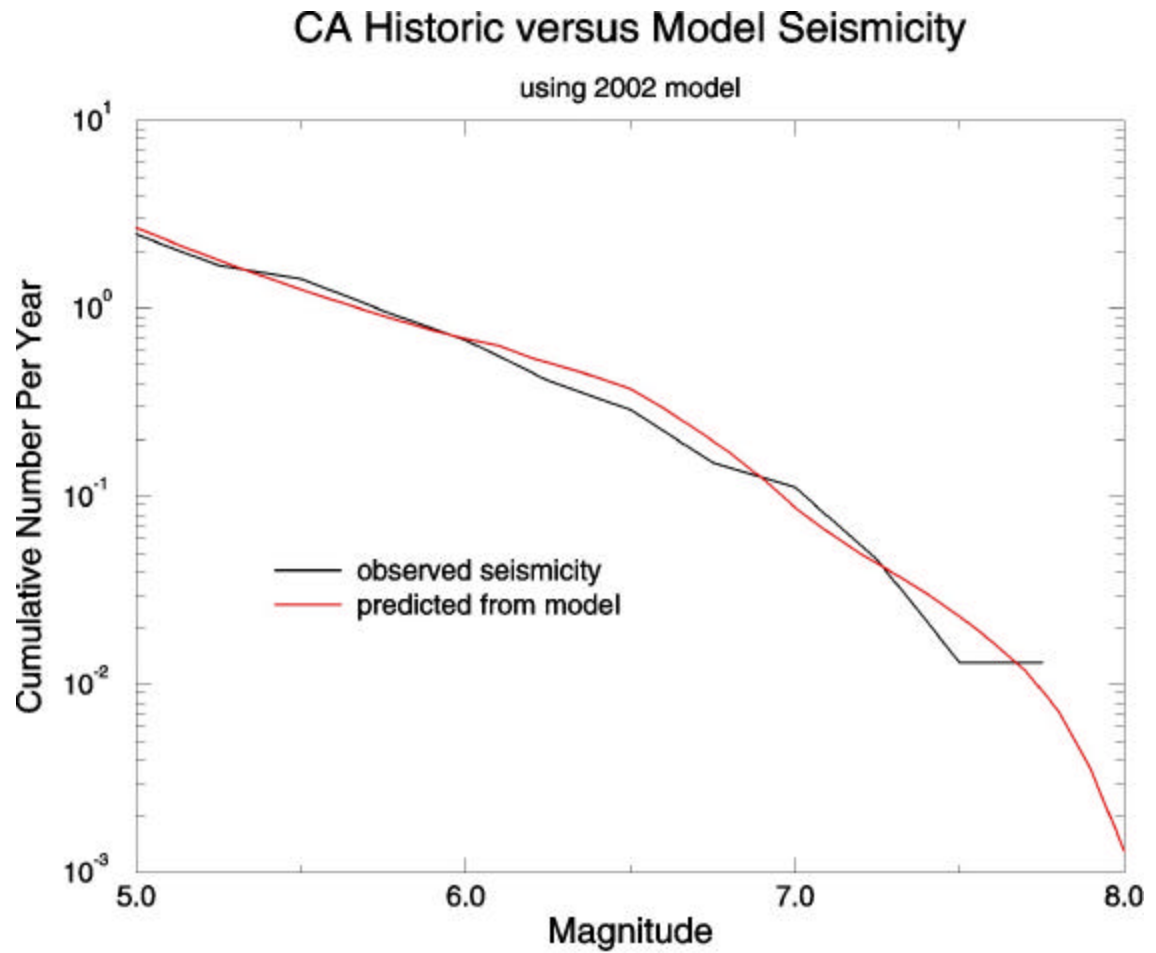


Figure 6. Comparison of predicted and historic seismicity rates for most of California.

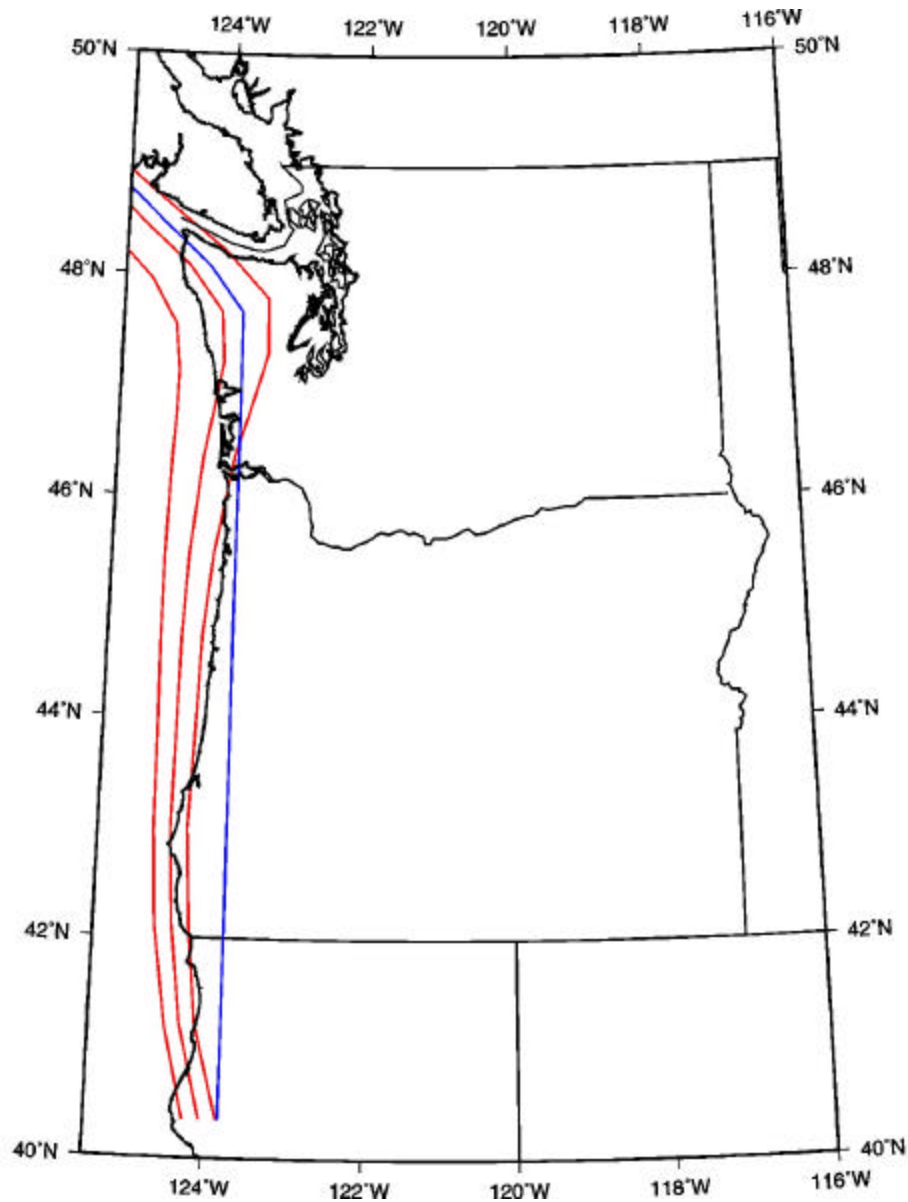


Figure 7. Configurations used in the 2002 maps for the eastern edge of the rupture zone for the Cascadia subduction zone. Red traces are (from west to east) the base of the elastic zone, the mid point between elastic and transition bases, and the base of the transition zone from Flick et al. (1997). Blue trace is a modification to the eastern edge of the rupture zone used in the 1996 maps, with a bend to the northwest at the northern end.

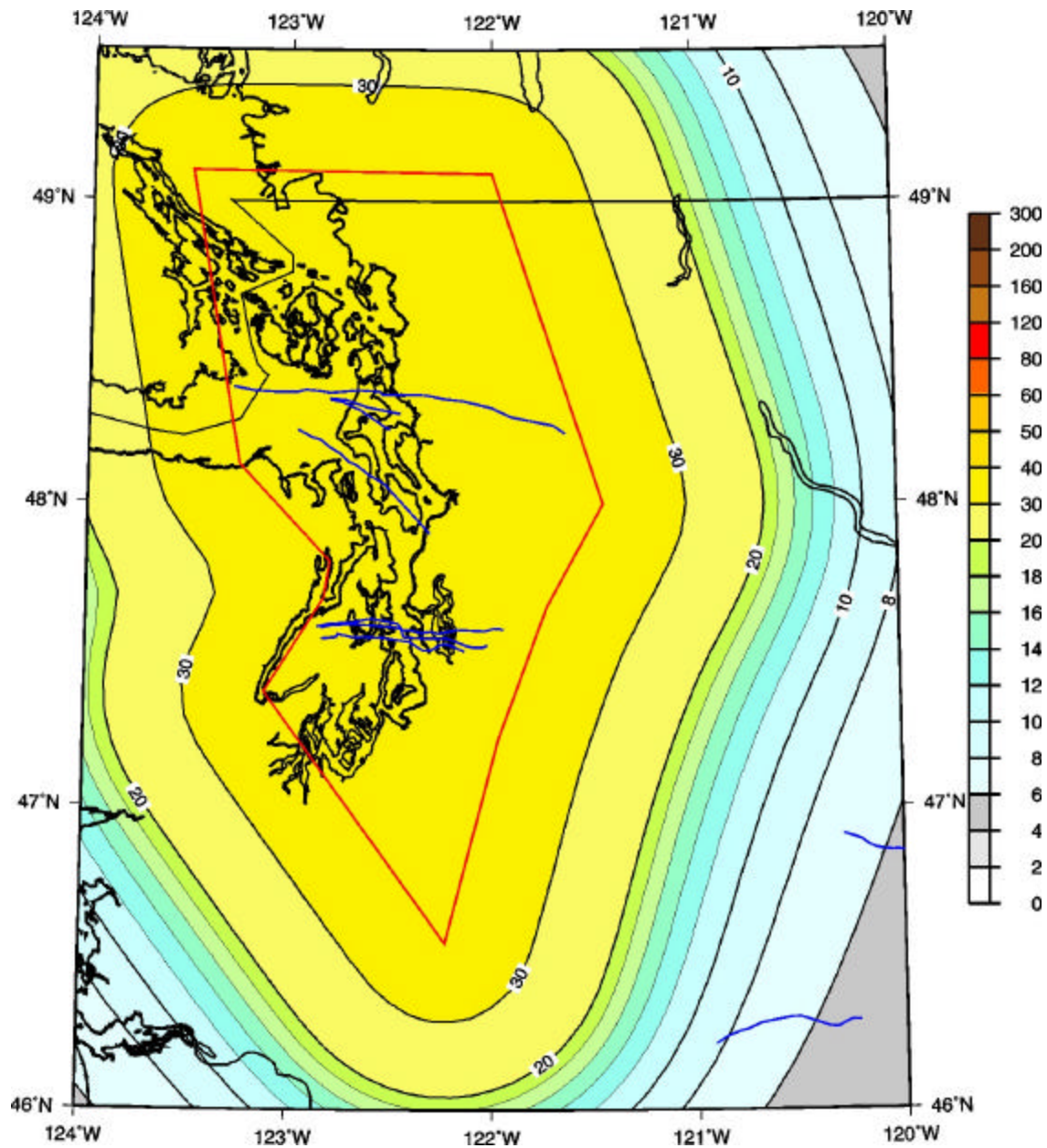


Figure 8. Outline (red) of Puget Lowland areal zone used in 2002 maps, with the PGA values (%g) for 2% probability of exceedance in 50 years calculated using only this zone. Blue traces are faults used in the 2002 maps.

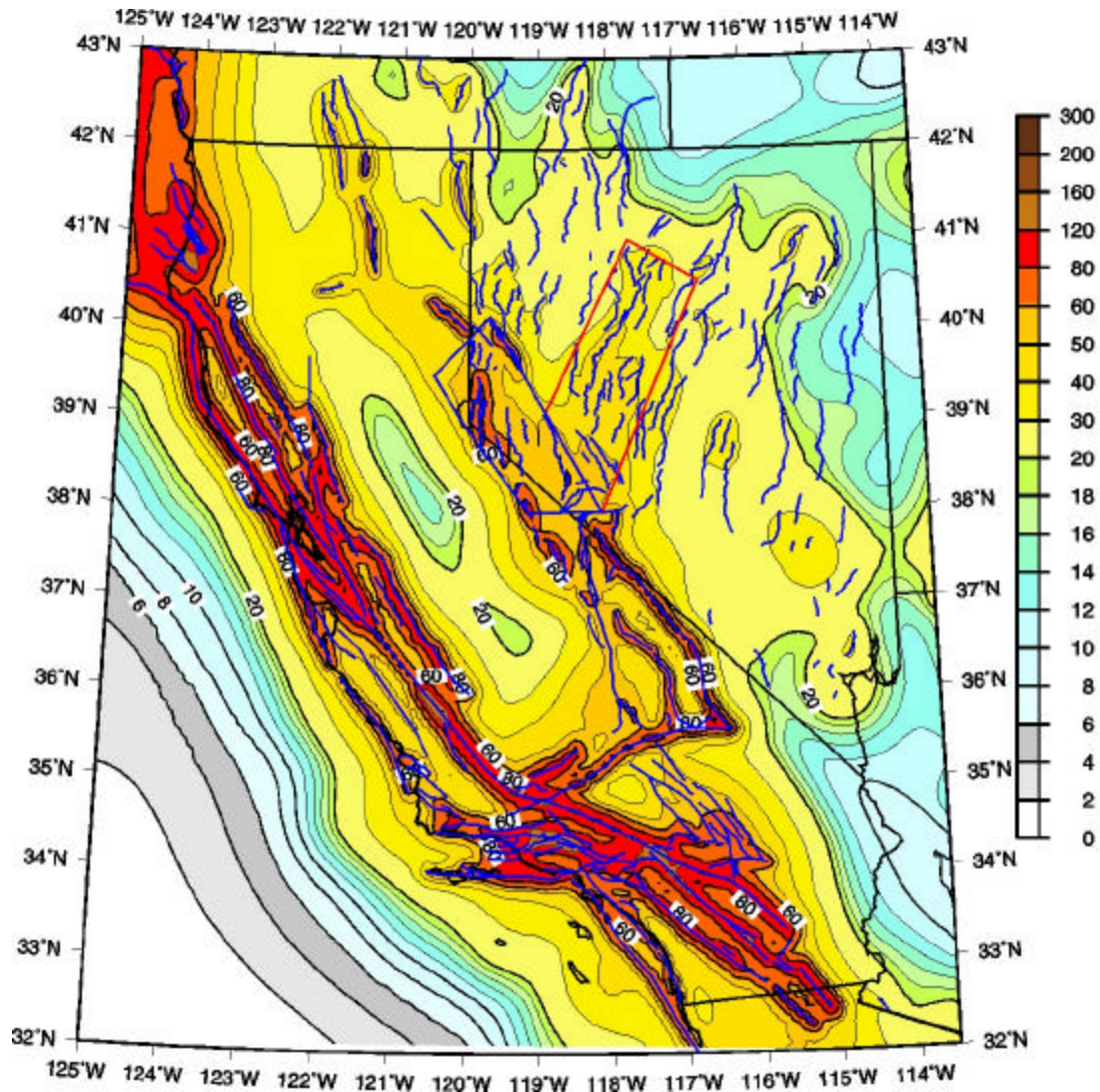


Figure 9. Map of PGA (%g) with 2% probability of exceedance in 50 years, showing outline of Mmax zone for the Central Nevada seismic zone (red box), outline of one of the shear zones (blue box), and fault traces (blue).

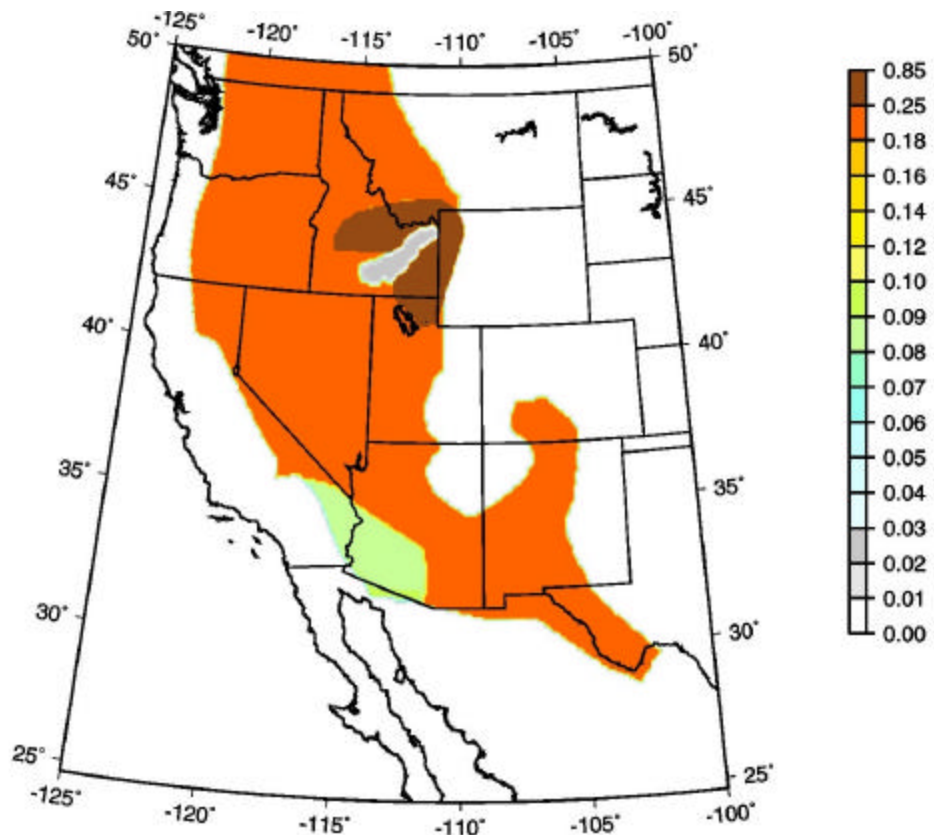


Figure 10. Background zones for the western U.S. used for the 2002 maps. The colors correspond to the seismicity rate used for each grid cell for that zone.

## Appendix A: Cascade Models for Southern San Andreas (Cholame -Coachella)

This Appendix describes the two new multiple-segment models we have developed for the southern San Andreas fault, defined here as extending from the Cholame segment through the Coachella segment. All recurrence rates are specified per year; all exponents are base 10.

### Model 1.

Three moment-balanced models are used:

- a. rupture from Cholame through Coachella
- b. rupture from Cholame through Mojave and rupture from San Bernardino through Coachella
- c. single-segment ruptures: Cholame, Carrizo, Mojave, San Bernardino, Coachella

For each model (a,b,c), magnitudes were determined by averaging the results from Ellsworth (in WGCEP, 2002) and Hanks and Bakun (2002) magnitude-area relations. Moment rates were calculated from slip rates and fault areas. Recurrence rates were determined by dividing the appropriate moment rate by the seismic moment of that scenario earthquake (e.g., Cholame-Mojave rupture for model b).

Weights were assigned to models a,b,c so that the total rates of large earthquakes on a given segments were roughly consistent with observed paleoseismic rates. We found that the single-segment model (model c) must have low weight since it predicted rates much higher than observed paleoseismic rates. Model a must have substantial weight in order to lower the total rates. We chose weights of 0.4, 0.5, and 0.1 for models a, b, and c, respectively. This gave a total rate (per year) on Carrizo of  $6.2e-3$ , Mojave  $6.3e-3$ , San Bernardino  $4.9e-3$ , and Coachella  $5.2e-3$ . The Carrizo rate is a bit higher than the observed  $4.7e-3$  rate.

Note that the total moment rate from Cholame through Coachella should be  $5.9e18$  dyne cm, given the slip rates and areas. Each model (a,b,c) satisfies this moment as, of course, does the weighted average model.

### Model 2.

In this model, we assume that the Carrizo segment only ruptures in 1857 type earthquakes (Cholame through Mojave). We use a paleoseismic recurrence rate of  $4.7e-3$  (SCEC Phase 2 Report: Working Group on California Earthquake Probabilities, 1995) for 1857 type events. For the Cholame segment, we assume a characteristic displacement per event of 4.75m (SCEC Phase 2 Report WGCEP, 1995). The 1857-type recurrence rate of  $4.7e-3$  times 4.75m yields 22 mm/yr. This leaves 12 mm/yr needed to achieve the total slip rate of 34 mm/yr. Assuming 4.75m per event requires a recurrence rate of  $2.5e-3$  to achieve 12 mm/yr. The magnitude for the Cholame segment is problematic. A 4.75m average displacement, along with the area of the Cholame segment, gives a seismic moment that corresponds to a M7.3 earthquake.

For the Mojave segment we use a characteristic displacement of 4.4m/event (SCEC Phase 2 Report WGCEP, 1995). The 1857 rate of  $4.7e-3$  times 4.4m yields 21 mm/yr. This leaves 9 mm/yr needed to achieve the total slip rate of 30 mm/yr. Given

4.4m per event, the 9 mm/yr requires a recurrence rate of  $2.05 \times 10^{-3}$ . The slip per event of 4.4m and the area of this segment yields a moment that corresponds to M7.4.

For San Bernardino through Coachella rupture, we find a magnitude of 7.7 from the fault area and either the Ellsworth or Hanks and Bakun (2002) relations. Given the moment rate on this rupture derived from the slip rate and area, we find a recurrence rate of  $5.5 \times 10^{-3}$ , similar to paleoseismic evidence. Using a single segment Coachella rupture would give a recurrence rate much higher than the observed paleoseismic rate.

Note that the total moment rate of model 2 is  $5.4 \times 10^{18}$  dyne cm, about 92% of that predicted.

## **Appendix B: Seismic Hazard Maps for the Conterminous U.S. for 2002**